In vivo pharmacodynamics of lactoferrin-coupled lipid nanocarriers for lung carcinoma: intravenous versus powder for inhalation

Dina M. Gaber (dinagaber@aast.edu)

Arab Academy for Science Technology and Maritime Transport College of Maritime Transport and Technology

Noha Nafee

College of Pharmacy: Kuwait University Faculty of Pharmacy

Ahmed O. Elzoghby

Alexandria University Faculty of Pharmacy

Maged W. Helmy

Damanhour University Faculty of Pharmacy

Osama Y. Abdallah

Alexandria University Faculty of Pharmacy

Research Article

Keywords: Cancer, Lactoferrin, tissue distribution, inhalable microparticles

Posted Date: October 17th, 2023

DOI: https://doi.org/10.21203/rs.3.rs-3334664/v1

Abstract

Lung carcinoma characterized by high mortality rate and poor prognosis; the efficacy of drug delivery should improve drug exposure at the targeted site. this study aims at evaluating lactoferrin role as targeting ligand besides the administration route impact on tissue deposition and organ distribution.

Lactoferrin (Lf)-coupled/uncoupled solid lipid nanoparticles (SLNs) were loaded with myricetin-phospholipid-complex (MYR-PH-CPX). Following physicochemical characterization, *in-vitro* antitumor activity and cellular uptake were investigated in A549-cell line. *In-vivo* deposition and biodistribution of fluorescently-labeled inhalable microparticles (with/without-Lf) were compared to intravenously administered fluorescently-labeled-SLNs (with/without-Lf) in mice.

Lf-coupled-SLNs (98.59±0.47 nm), showed high entrapment efficiency (95.3±0.5%) and prolonged drug release. The *in-vitro* antitumor study showed reduction in IC_{50} for Lf-coupled-SLNs by ~2-and 3.5-fold relative to uncoupled-SLNs and MYR-PH-CPX, respectively confirming Lf role in enhancing antitumor activity by boosting cells internalization in shorter time. Furthermore, 3D-time laps confocal imaging showed that labeled-Lf-coupled-SLNs had a higher rate and extent of uptake in A549-cells compared to uncoupled-SLNs and free dye. *In-vivo* biodistribution proved that Lf enhanced pulmonary deposition of inhaled SLNs (~1.5 fold) and limited migration to the other organs within 6h relative to intravenous. Conclusively, local administration is superior due to less drug clearance resulting in lower toxicity accompanied by systemic application.

1. Introduction

Successful drug delivery depends on the development of formulations that are capable of improving the therapeutic index of drugs by increasing their concentration specifically at desired target sites or organs while restricting their entrance to the non-target organ, thus minimizing toxic effects [1, 2]. Thus, active targeting is kind of smart drug delivery system which employs a deliberately modified drug, drug-carrier molecule capable of recognizing and interacting with a specific cell, tissue or organ. These ligands-based systems for targeting are advantageous over other systems because they minimize the chance of serum-protein binding and opsonization on their surface[3]. Moreover, active targeting is accomplished by attachment of specific molecules on the carrier's surface, which enhance the binding and interactions with antigens or receptors expressed on specific cell populations [4, 5].

It was reported that lung targeting in specific "the deep lung" confronts a crucial challenge, namely the premature mucocilliary clearance. Ligand-anchored drug delivery system aim at achieving enhanced site-specific drug delivery as well as reduced reticular endothelial system (RES) uptake [6, 7]. However, the clinical success of such an approach depends on the selection of appropriate ligands lacking immunogenic potential with the ability to mediate cargo internalization by the target cell [8]. With this concern in mind, lactoferrin (Lf) may function as a ligand suitable for coupling with SLNs, generating a promising drug delivery system to the lungs[9].

Lactoferrin (Lf), is an iron-binding glycoprotein of the transferrin family that was discovered in mammarian secretions in 1939. Lf is a protein with a huge molecular weight of 80 KDa that is made up of 700 amino acids that are held together by disulfide bonds [10]. There are 3 isoforms for Lf: α isoform is the iron-binding one, whereas the non-iron binding isoforms are β and γ possessing ribonuclease activity [11]. Lactoferrin's biological roles have been found to include anticancer, antibacterial, antiviral, antifungal, anti-inflammatory, and immune-regulatory properties [12]. Lf was reported to exhibit anti-cancer efficacy via different mechanisms [13, 14].Some studies showed that Bovine Lf has been found to significantly inhibit colon, esophagus, lung and bladder carcinogenesis in rats when administered orally in the post-initiation stages [15]. Furthermore, it has the inherent capability to provoke apoptosis and hinder cancer cell proliferation. Lf also promotes restoration of leucocytes and erythrocytes after chemotherapy [16]. The biological properties of Lf are mediated by specific receptors on the surface of target cells which are expressed on the apical surface of bronchial epithelial cells (BEAS-2B) and this conception is utilized to achieve targeted drug delivery to the lungs [17].

Nevertheless, pulmonary delivery via inhalation is a common technique of drug administration to patients with a variety of lung diseases [18]. However, nanoparticulate delivery to the lungs appears to be problematic, as their nanosize increases their probability of exhalation before deposition [19]. Moreover, the high interparticulate forces may dominate resulting in uncontrolled aggregation and preventing de-aggregation upon aerosolization under the normal air flow rates in passive DPIs. Therefore, to successfully deliver nanoparticles by inhalation, they first have to be transformed into micro-scale nanocomposite structures having aerodynamic diameter between 1 and 5 μm [19].

Based on our previous research data [20], it was concluded that by preparing MYR-phospholipid complex (MYR-PH-CPX) and loading it in SLNs (MYR-CPX-SLNs) resulted in 5-fold increase in drug loading into NPs, 3-fold enhancement in antitumor activity. This was related to enhanced cellular uptake that was revealed by confocal imaging and doubled fluorescence intensity [20].

For superior anti-cancer potential, this study attempts to evaluate the role of lactoferrin as a lung targeting ligand in augmenting antitumor activity and cellular uptake for effective management of non-small cell lung cancer (NSCLC). Thus, the aim of this study is to develop Lf-coupled SLNs loaded with MYR phospholipid complex (Lf-MYR-CPX-SLNs). Concrete milestones comprise the potential of Lf-coupled, fluorescently-labeled nanocarriers in selective intracellular delivery of the cargo into adenocarcinomic human alveolar cells (examined by confocal laser scanning microscopy), which would be translated to more efficacious antitumor activity relative to uncoupled SLNs (MYR-CPX-SLNs) and free MYR. Inhalable spray dried fluorescently-labeled microparticles designed for inhalation as dry powder inhaler (DPI) (SD-Cou MP) were prepared.

In addition, in vivo biodistribution and lung residence time were monitored following local and systemic administration (IV) in mice. Thus, deposition of all formulations will be performed. All studies comprised investigation of free dye and non-targeted SLNs/MP as controls.

2. Materials and methods

2.1. Materials

High purity myricetin was purchased from Shanghai Tauto Biotech Co. Ltd, Shanghai, China. Lipids like Gelucire 50/13 and Compritol 888 ATO, were gift samples from Gattefosse, Lyon, France. Soybean phosphatidylcholine (Lipoid® S 100) (purity > 96%) was purchased from Lipoid GmbH, Ludwigshafen, Germany. Coumarin-6 was acquired from Polysciences Europe GmbH, Hirschberg, Germany. Hoechst 33342, blue fluorescent stain specific for DNA (i.e., nuclei of eukaryotic cells), was received from Thermo Fisher Scientific, USA. Lactoferrin was kindly provided from Sigma Aldrich, Schnelldorf, Germany. O-phosphoric acid and Methanol (HPLC grade) were obtained from Merk, Massachusetts, USA. Lung epithelial cancer cell line A549 and Dulbecco's modified eagle medium (DMEM) and fetal bovine serum (FBS) were purchased from the American Type Culture Collection, ATCC, USA and Gibco, Basel, Switzerland, respectively. Sodium sulfite was purchased from El-Nasr Pharmaceutical Co., Cairo, Egypt.

2.2. Methods

2.2.1. Formulations of delivery systems

2.2.1.1. Preparation of MYR-CPX-SLNs with/ without Lf for studying antitumor activity

MYR-PH-CPX loaded SLNs were prepared as previously reported in details by Nafee *et al.*[20]. The formulation contains MYR, G50/13, Cp, Lipoid S100 in concentrations 0.1, 2.5, 0.5 and 1 % wv, respectively, per SLNs dispersion. A dispersion of MYR and Lipoid S 100 in molar ratio (1:4) was dissolved in 1:1 (ethanol : acetone) followed by solvent evaporation to form MYR-PH-CPX. The later was loaded into melted lipids at 55°C in a water bath, and then preheated purified aqueous phase was added slowly under magnetic stirring. Further, the nano dispersion was homogenized and sonicated in water bath for 15 mins each step at the same temperature range. Finally, SLNs were solidified by cooling under stirring at low speed. Further, SLNs were decorated with 1% w/v Lf as a targeting ligand (Lf-MYR-CPX-SLNs) after trying 10 different concentrations from (0.2-6% w/v) (Table 1). In brief, Lf stock aqueous solution (10 % wv) was added dropwise to 10 ml of SLNs dispersion under continuous stirring for 45 min at 300 rpm at room temperature to ensure stabilization.

2.2.1.2. Preparation of fluorescently labeled-SLNs with/ without Lf for uptake and biodistribution studies.

Coumarin-6 was loaded in to SLNs to allow their visualization using confocal laser scanning microscope (λ_{ex} 450 nm, λ_{em} 505 nm). SLNs were formulated as mentioned above while replacing MYR with coumarin-6 (10 µg/ml of SLNs dispersion). After that, SLNs were functionalized with lactoferrin in

concentration 1% w/v. Both formulations (Lf-Cou-SLNs and Cou-SLNs) contain G50/13, Cp and Lipoid S100 in concentrations 2.5, 0.5 and 1% w/v, respectively per SLNs dispersion.

2.2.1.3. Preparation of nano-embedded spray dried microparticles (SD-MPs) for inhalation

As we previously reported [21] that the prepared MYR-CPX-SLNs dispersion was spray dried in the presence of carbohydrate carrier system. To choose the optimum formulation, different carrier system blends of mannitol, maltodextrin and leucine at a constant carrier: SLNs weight ratio of 3:1 were tried. Detailed compositions of different spray dried MYR microparticles formulations (SD-MP1-SD-MP4) are displayed in Table 2. Further, Cou 6-SLNs eithercoupled with Lf or not were spray dried in presence of the optimized carrier system to prepare fluorescently labeled SD-MPs denoted as (SD-Lf-Cou MP/ SD-Cou MP), respectively for the *in vivo*deposition experiment.

Table 1: Composition of Lf-coupled and uncoupled MYR-CPX-SLNs

Concentration of lactoferrin/ SLNs dispersion (% w/v)					
Formula code	Drug	Lipids		Phospholipid	Targeting ligand
	MYR	G 50/13	Cp 888	Lipoid s 100	(Lf)
MYR-CPX-SLNs	0.1	2.5	0.5	1	___
Lf- MYR- CPX -SLNs-1					0.2
Lf- MYR- CPX -SLNs-2					0.4
Lf- MYR- CPX -SLNs-3					0.5
Lf- MYR- CPX -SLNs-4					0.6
Lf- MYR- CPX -SLNs-5					0.8
Lf- MYR- CPX -SLNs -6*					1
Lf- MYR- CPX -SLNs -7					1.6
Lf- MYR- CPX -SLNs -8					2
Lf- MYR- CPX -SLNs -9					4
Lf- MYR- CPX -SLNs-10					6

Table 2: Composition of spray dried microparticles

Carrier: MYR-CPX-SLNs (w: w) weight ratio				
SD-MPs	Mannitol	Maltodextrin	Leucine	MYR-CPX- SLNs
SD-MP1	3	___	___	1
SD-MP2	2	___	1	1
SD-MP3	1.5	0.75	0.75	1
SD-MP4	0.75	1.5	0.75	1

Spray drying was performed by Spray Dryer B-90 (Büchi, Flawil, Switzerland). The conditions were adjusted at 110 and 55°C as inlet and outlet temperatures, respectively, 100% aspiration, 15% pump rate and 320 L/h air flow rate. The SD-MPs were collected gently by scrapper and stored in airtight amber glass vials in a desiccator at room temperature for further investigations.

2.2.2. Characterization of delivery systems

2.2.2.1. Colloidal properties, Morphology

Malvern Instrument Nano- Zetasizer Malvern, UK was used to determine the particle size distribution and surface charge of previously diluted NPs with water for injection as reported by Gaber *et al.*[20, 21]. The results were expressed as the average and standard deviation of three measurements. Moreover, the structure of SLNs was visualized by transmission electron microscopy TEM, model JEM-100CX (JEOL, Japan) after negative staining with uranyl acetate.

2.2.2.2. Confirmation of Lf coupling efficiency

To qualitatively confirm the Lf coupling efficiency to SLNs, the IR spectra of Lf, MYR-CPX-SLNs and Lf-MYR-CPX-SLNs, (F6) containing 1% w/v Lf, were obtained using FTIR spectroscopy (Perkin Elmer, USA) to confirm Lf coupling to SLNs surface as previously detailed [20].

To evaluate the total Lf concentration in SLN dispersion, Lf-MYR-CPX-SLNs (F6) were used, whereas to quantify the amount of Lf typically bound to SLNs, the nanodispersion was purified by centrifugal ultrafiltration using Centrisart-I® (MWCO 100,000) (Sartorious Lab Ltd., Stonehouse, United Kingdom); unbound Lf was determined in the supernatant by Bradford assay. Briefly, 0.1 ml of either Lf-MYR-CPX-SLNs (F6) or supernatant was transferred to 10 ml volumetric flask with 1 ml coomassie blue G dye solution (10% w/v), then the volume was modified accurately to 10 ml with purified water followed by 200-folds dilution. Lf concentration was examined by measuring the absorbance at 595 nm against a blank containing the same quantity of dye. Plain SLNs were also measured as control to eliminate any sort of interference from the nanosystem with the assay.

2.2.2.3. Entrapment efficiency and in vitro release study

The encapsulation efficiency of both Lf coupled/ un coupled SLNs was measured directly by means of Centrisart-I®, MWCO 20 kDa[22] as previously described by Gaber *et al.*[21] where, The entrapped MYR had been extracted by methanol from purified loaded SLNs after centrifugation at 4000 rpm, for 15 min, followed by quantification using aforementioned published validated HPLC method [21]. While, the release experiment was carried out as previously published[20] using Dialysis method in hydroethanolic dissolution medium (1:1 v/v), 50 ml. the shaker water bath was calibrated at 100 strokes/ min and 37°C ±0.5. At different time intervals (1, 2, 4, 6, 8 and 24 h) a sample of 0.2 ml was removed and replaced with same volume of pre warmed fresh medium. Then % of drug release was determined by HPLC [21].

2.2.2.4. Microparticles characterization

The prepared spray dried microparticles were characterized in terms of; size, morphology, yield and % drug recovery as detailed in the supplementary material section. Further, the flow properties were assessed in terms of calculating angle of repose, Carr's index (CI) and Hausner ratio (HR), as described in the supplementary material section.

Drug-excipients incompatibility studies were performed in terms of thermal behavior by differential scanning calorimetry (DSC) and Fourier Transform Infrared (FTIR) Spectroscopy. Samples assessed encompassed MYR, mannitol, maltodextrin, leucine, and selected SD-MYR MP formulations (SD-MP2, SD-MP3). The tests in details are described in the supplementary material section.

Furthermore, *in vitro* aerosol deposition was evaluated as previously reported [20]. The test was carried out by using the Aerolizer® as the inhaler device connected to the Andresen Cascade Impinger (ACI). Where a capsule containing 20 mg of SD-MP was placed in the aerolizer that is attached to neck of impinger. Then the capsule was pierced to allow the powder to flow in the impinger at 28.3 l/min flow rate. Then the powder at each stage from S0-S7 was collected and analyzed by HPLC as previously published. The in vitro aerosolization properties were expressed as previously published[20] in terms of; mass median aerodynamic diameter (MMAD), emitted dose (ED), emitted dose fraction (EF), fine particle fraction (FPF) and geometrical standard deviation (GSD).

2.2.3. *In vitro* assessment on cell culture model

2.2.3.1. Antitumor activity of Lf coupled and uncoupled MYR-CPX-SLNs

As a proof of concept for the role of Lf in enhancing antitumor activity, A549 lung carcinoma cells were used using MTT assay. Briefly, in a Corning 96-well plate A 549 cells at concentration $5x10^4$ cell/well were incubated 24 h with MYR-PH CPX, Lf-coupled and uncoupled SLNs loaded with MYR-PH-CPX. Samples were diluted with DMEM supplemented with 0.025% sodium sulfite to achieve eight different concentrations of MYR (10, 20, 40, 50, 60, 80, 100 and 200 μM). Afterwards, washing step with fresh medium was done and MTT reagent was added for 4 h followed by another washing step then DMSO was added to solubilize formazan crystals for 10 min at 37 °C. Then, microplate reader (SunRise, TECAN Inc, USA) was used to determine the amount of the solubilized formazan crystals spectrophotometry at 570 nm. The percentage of cell viability relative to control cells incubated with culture medium only was calculated by the following equation and IC 50% was estimated from the graph [20, 21].

$$\% \text{ Cell viability} = \left[\frac{\mathrm{A(Test)} - \mathrm{A(Negativecontrol)}}{\mathrm{A(Positivecontrol)} - \mathrm{A(Negativecontrol)}}\right] * 100 \quad \text{..... Eq. 1}$$

2.2.3.2. Localization and Cellular uptake in A549 cells

The cellular uptake of both Lf-coupled and uncoupled Cou 6-labeled SLNs and free coumarin toward A549 cells was measured through confocal laser scanning microscopy to test effect of targeting ligand on uptake efficiency. In brief, A549 cells were seeded on IbiTreat ® 8- chamber slides at density 12,500

cells/ml. On the next day, samples were incubated with cells at concentration equivalent to 6 ng Cou for 4 and 24h. After washing cells with PBS and then fixed with neutral formalin, the nuclei were stained blue with Höchst 33342 and visualized by CLSM. The rest of procedure had been processed as previously reported in our previous work [20].

2.2.4. *In vivo* pharmacodynamics following *IV* vs inhalation.

2.2.4.1. Experimental animals and study protocol

The *in vivo* biodistribution study was applied to distinguish between the distribution pattern of actively- and passively targeted formulations. Besides, the efficiency of pulmonary drug deposition following inhalation was compared versus intravenous injection. This study was performed on swiss albino male mice 4–5 weeks old with 15–20 g weight. The experimental protocol was approved via the Animal Care and Use Committee of the Faculty of Pharmacy, Alexandria University as illustrated in the Supplementary data. Mice have been kept at room temperature (25 ℃) and 50% relative humidity and then housed in stainless-steel cord mesh cages. Mice were randomly categorized into 6 groups (4 mice/ group) and fasted overnight with no access restriction to water before treatment. Group (1) - mice receiving normal saline containing 313 ng free Coumarin 6, group (2) - mice were IV injected with NP suspension (Cou-SLNs) equivalent to 313 ng Cou 6 and group (3) mice were I.V injected with NP suspension (Lf-Cou-SLNs) equivalent to 313 ng Cou 6. The Intravenous injection was performed via tail vein with a 0.5 ml syringe with a tip of 0.3x12 mm.

On the other hand, A DP-4M insufflator (Penn-Century Inc., Philadelphia, PA, USA) had been used to deliver the respirable SD-MP. The insufflator was weighed prior to powder filling and following powder administration to determine the delivered dose. Powder administration was carried out by placing the end of the insufflator tube near the carina (first bifurcation of the pulmonary tract) to ensure that the dose of powder could reach deep into the lung. For powder delivery, 0.25 ml of air was puffed through the DP-4M device [23]. The mice were positioned in 90˚ angle and restrained by hand. Group (4) - received a dose 5 mg SD inhalable microspheres (SD-Free dye MP) containing 313 ng free Cou, Group (5) & (6) – animals were delivered 5 mg SD inhalable microparticles containing 1.25 mg Cou-SLNs (SD-Cou MP) and 6 mg SD inhalable microspheres containing 1.5 mg Lf-Cou-SLNs (SD-Lf-Cou MP) (equivalent to 313 ng Cou), respectively. Groups 1 and 4 were kept as control that acquired free dye.

2.2.4.2. Biodistribution study

At 1 and 6 h post administration, two mice from each category were sacrificed, and coronary heart perfusion was done with neutral formalin (10% in saline) as fixative [24]. Afterwards, organs (Liver, kidney, lung, spleen and brain) were collected and stored in 10% neutral formalin.

After fixation step, tissues of 2–3 mm thickness from every organ had been trimmed with a scalpel and located in a tissue cassette. Tissues in cassettes have been processed into paraffin, embedded in a

paraffin block, sectioned on a microtome to a thickness of 2 µm, placed on a microscope slide, following standard histology techniques.

2.2.4.3. Fluorescence microscopy

Fluorescence microscopy was chosen to localize coumarin-6 in distinct tissues. Slices of thickness (± 2 mm) of various tissues had been fixed in sample holder and covered with a glass cover slip for examination. Two slides from each tissue containing 2 different sections (total = 4 sections) were analyzed through fluorescent microscope (Olympus BX 41, Olympus America Inc., Mellville, NY, USA) supplied with planachromat N 20X and 40X Objective Lenses. The NPs were depicted as green color, then processed with *Image J* program to A cut-out value of 800*600 pixels (approximately 480 mm^2) was selected. Three screenshots from different parts of each section were analyzed [25]. The fluorescence microscope imaging was implemented at the Center of Excellence for Research in Regenerative Medicine and its Applications (CERRMA, Faculty of Medicine, Alexandria University, Alexandria, Egypt).

2.3. Statistical analysis

The results were reported as the mean of independent experiments ± standard deviation of. The one-way and two-way analysis of variance (ANOVA) tests were performed to determine the degree of significance, with a p-value of < 0.05 being statistically significant.

3. Results and Discussion

1. Lf coupled *versus* uncoupled SLNs for targeting lung cancer

1.1 Colloidal properties of targeted SLNs and Morphology

The size measurements indicated gradual increase in diameter from 75.28 to 120 nm with an increase in concentration of Lf from 0 to 4 %w/v, Formula F1-F9, Figure 1A, together with a corresponding increase in PDI. This change in size might be allocated to Lf attachment on the surface of NPs. Our results were consistent with those of Shilpi *et al*. [15] who reported an increase in SLN size by 35 nm when Lf was coupled to rifampicin-loaded SLNs, to achieve drug targeted delivery to the lungs for tuberculosis treatment. Similarly, coumarin-6 SLNs were 66.3±0.91 and 81.16± 0.97 nm in diameter with PDI of 0.216 and 0.318, for Cou-SLNs and Lf-Cou-SLNs, respectively.

The zeta potential of MYR-CPX-SLNs was (-26.5±4.38 mV), while, for Lf-coupled SLNs the ZP values are shifted from negative to positive by increasing Lf conc. ranging from -17.7±2.73 (F1) to 0.6±0.66 mV (F10) containing 6% w/v Lf. This change could be due to the presence of positively charged groups of amines groups of Lf which is covering SLNs' surface (Figure 1B) [27]. The reverted weak ZP reflects the doubling in PS that can be attributed to SLN agglomeration.

The surface morphology for both targeted (Lf-MYR-CPX-SLNs) and non-targeted SLNs (MYR-CPS-SLNs) appeared spherical with smooth surface as the TEM photomicrographs show (Figure 1C) while MYR-PH-

CPX showed irregular vesicular structure as previously reported [21]. Interestingly, ligand-coupled SLNs (F6) were darker in accordance with photomicrographs were obtained by Shilpi *et al.*[15].

1.2 Confirmation and quantification of Lf coupling to SLNs

SLNs were loaded with MYR-PH complex and prepared by the hot homogenization technique as reported by Gaber *et al.*[21]. Lf was attached to SLNs via electrostatic interaction between anionic SLNs and cationic Lf.

Lactoferrin coupling efficiency to SLNs was confirmed by FT-IR. The FT-IR analysis of free Lf showed the distinctive protein band peaks; at 3288 cm^{-1} represents –N–H stretching of the amide I at 1635.815 cm^{-1} due to C=O stretching vibration of the peptide group and amide II at 1508.298 cm^{-1} due to N–H bending with contribution of C–N stretching vibrations. The amide peak has disappeared in the spectra of Lf-MYR-CPX-SLNs which was considered as further confirmation of Lf attachment and there was no shift in peak positions compared with free Lf (Figure 2). Similar observations were noticed by Yao *et al.* [26] who developed, bovine Lf-loaded Liposomes and SLNs.

Further, from Bradford test, in case of Lf-MYR-CPX-SLNs (F6) the concentration of unbound Lf was 0.47 mg/ml reflecting Lf coupling efficiency of 95.17 %.

1.3 Drug entrapment efficiency and *in vitro* release study

MYR entrapment efficiency was 97.9±0.14% to 95.3±0.5% for uncoupled and Lf-coupled SLNs (F6), respectively. This slight decrease in entrapment efficiency (%EE) may be attributed to slight leaching of the drug during the incubation process at the time of Lf attached with SLNs. Similarly, the encapsulation of Cou-6 in SLNs was found to be promising (96 and 98.4%) for both Lf-coupled and non-non coupled SLNs, respectively. These results highlighted the ability of these NPs (Cou-SLNs/ Lf-Cou-SLNs) for diagnostic and cellular trafficking purposes.

The in vitro drug release from Lf coupled and uncoupled MYR-CPX-SLNs was studied using the dialysis technique. The percent MYR release was recorded to be 71.5±1.33 % and 67.7±2.01% from MYR-CPX-SLNs and Lf-MYR-CPX-SLNs, respectively (Figure 1D). Lf might provide considerable shielding on the NP surface. Similar release behavior was reported for rifampicin and paclitaxel release from uncoupled and Lf-coupled SLNs [15,27] as well as methotrexate release from lactoferrin–dendrimer conjugates (Lf-PPI) and plain dendrimer (PPI) [28].

.2 *In vitro* assessment on cell culture models

2.1 Anti-tumor activity

Previous data revealed 33% reduction in IC_{50} for MYR-phospholipid complex instead of free MYR [20]. Herein, the antitumor activity of Lf-MYR-CPX-SLNs (F6) was explored relative to MYR-phospholipid

complex and MYR-CPX-SLNs.

Lf functionalized SLNs were found to exhibit significant superior growth inhibition of A549 cells *(Two-way, ANOVA, p =0.000002)* in comparison to non-functionalized SLNs and MYR-phospholipid complex. The viability profiles showed high % viability ranging from 60 to 89 % at low MYR concentration (20 μM), Figure 3. By comparing our results to results obtained by Rajendran *et al.* [29], who performed cytotoxicity study for MYR on A549 cells in concentration range from 20 to 315 μM. it was found that at low MYR content (20 μM), 92% cell viability was obtained which decreased by increasing the drug concentration and the obtained IC_{50} was 229 μM [29]. Further, gradual increase in concentration resulted in a corresponding reduction in viability to 10 % in case of Lf-MYR-CPX-SLNs compared to 43 % for MYR-phospholipid complex at 200 μM MYR concentration. Indeed, 2-3 fold lower IC_{50} value was recorded for Lf-functionalized SLNs (35.01 μM) compared to 67.29 and 113.8 μM for MYR-CPX-SLNs and MYR-phospholipid complex, respectively.

The potential toxicity of targeted SLNs might be attributed to improved cellular uptake via ligand–receptor interaction. These findings were in good agreement with research published by Pandey *et al.*[27] who reported that, Lf-coupled SLNs encapsulating paclitaxel (PTX) exhibited considerable higher cytotoxicity as compared to PTX-loaded SLNs. Further, PTX solution was found to be less cytotoxic and IC_{50} values were 7.5±0.4, 4.6±0.1 and 1.1±0.03 μg/ml for Free PTX solution, PTX-loaded plain SLNs and PTX-loaded Lf-coupled SLNs, respectively.

2.2 In vitro cellular uptake and colocalization studies

2.2.1 Effect of incubation time

The uptake of Cou-SLNs and Lf-Cou-SLNs as well as free dye solution in DMSO was investigated on A549 cells for 4 and 24 h by CLSM.

After 4 h incubation period, very weak green fluorescence comparable to control cells could be recognized in case of Cou-SLNs and free dye (Figure 4A). In comparison, Lf-Cou-SLNs exhibited distinct green spots even within this short incubation period.

Longer incubation with A549 cells (24 h) enabled better uptake of all samples including free dye, Cou-SLNs and Lf-Cou-SLNs (Figure 4A). Interestingly, stronger fluorescence signals denoting higher level of internalization could be depicted in case of Lf-Cou-SLNs. Nafee *et al.*[20] previously reported that the total fluorescence intensity of Cou-SLNs internalized was >2.5 times higher than that of free dye. Herein, Lf-Cou-SLNs showed ~ 4 folds higher fluorescence intensity in the cells than Cou-SLNs (Figure 4B)–confirming the direct effect of ligand targeting on cellular uptake.

2.2.2 Localization of labeled SLNs in A549 cells

In order to distinguish between surface binding of SLNs and concrete internalization, 3D time laps imaging was carried out allowing imaging of 40 stacks inside the cells in the z-direction along 14 µm (Figure 4C). The Z-stacks confirm particle localization inside the cells namely within the cytoplasm and seldom dispersed in the nuclei. Lf-Cou-SLNs could be clearly detected with intense green fluorescence intensity and sharper spots within the cell vicinity indicating their possible entrapment in intracellular vesicles. This reveals the vital role of active tumor targeting via ligand-receptor binding in improved cancer nanotherapeutics. Similarly, Liu *et al.*[30] demonstrated that, (RRWQW) a cell penetrating peptide obtained from bovine lactoferrin, was non-covalently complexed with plasmid DNA, is able to efficiently deliver the plasmid DNA into A549 cells.

3. Nano-embedded microparticles for inhalation (Physical characterization)

For better drug deposition deeply in the lung, the nanoparticles should be converted to microparticles to overcome clearance by exhalation. Thus, in this study a two-step process successfully prepared inhalable SD-MPs with aerodynamic diameter between 1 and 5 µm.

We previously formulated SD-MPs [20] by spray drying MYR-CPX-SLNs with carrier mixture consisting of mannitol: maltodextrin and L-leucin (1.5:0.5:0.75 %w/v) (SD-MP3). A prefect yield of 89% w/w of excellent flow powder was achieved with aerodynamic diameter 2.39 µM and drug recovery of 95% [20]. The aforementioned optimized formulation was selected for the current study.

Matrix formers namely sugars (mannitol) or polysaccharides (maltodextrin), were selected because of their ability to act as drying protectants for drugs during water removal process and to shape the MP modulating particle/particle interactions [31,32]. The amino acid L-leucine was added to act as an aerosolization enhancer forming a coat (shell) on the dry particle surface preventing any particle fusion and therefore preserving the individual MP as collected from the dryer [31]. Moreover, it was employed due to its powder dispersibility enhancing effect as previously reported in many studies [32,33].

3.1 Percentage of yield recovered and drug content

It was found that, the % yield of spray-dried powder varied between 28.75 - 89.05% w/w during spray drying processing as illustrated in the supplementary material, Nevertheless, by combining maltodextrin with mannitol in either SD-MP3 or SD-MP4, an increase in the yield was slightly significant when compared to SD-MP2, (*One-way ANOVA, $p < 0.05$*) (Table S.1- supplementary material). This observation was in accordance with previous literature demonstrating that the presence of dextran as an example of oligosaccharides with mannitol. It was found that dextran was able to suppress the shrinkage and particles collapse due to the change in glass transition temperature T_g (collapse temperature). This is attributed to suffering of mannitol from low T_g besides its rubbery state might result in sticking to the spray dryer [32]. Similarly, a study reported by Kumar *et al.* [34] where, a combination of a low molecular weight sugar with a high molecular weight one was used to achieve higher spray drying yields. Further, MYR content in the different formulations (SD-MP1 to SD-MP4) ranged from 90.5 to 95.15 % (Table S.1-

supplementary material). Thus, the active ingredient seemed to be uniformly distributed in the different powder formulations.

3.2 Particle size measurement

The size of microparticles (SD-MP1 to SD-MP4), (Dv50) was remarkably small ranging from 4.5 to 6.90 µm indicating their suitability for lung deposition. The span values (1.24 – 1.84) reflect the narrow particle size distribution as depicted in (Table S.2-supplementary material).

3.3 Morphological characterization

SEM photomicrographs of raw MYR, and SD-MPs powders (SD-MP1 to SD-MP4) were demonstrated in Figure 5A-E. The scanning electron micrograph of raw MYR (Figure 5A) revealed the presence of large crystals aggregated together with a particle size that is too large for inhalation. Spray drying MYR-CPX-SLNs with different water-soluble matrix formers resulted in change in the particle appearance. It was depicted that, presence of mannitol in (SD-MP1) showed separated spherical particles with moderately corrugated surface (Figure 5B), whereas SEM images of leucine-containing particles (SD-MP2) revealed the enhancement in both surface roughness and corrugation (Figure 5C). By virtue of leucine hydrophobicity it probably acted as a water repellent and thus reduced moisture uptake by sugars, reducing their particle cohesiveness [32,35]. By combining the high molecular weight maltodextrin with the low molecular mannitol in either SD-MP3 or SD-MP4, spherical particles with less corrugated surface were obtained (Figures D-E). The use of different ratios between mannitol and maltodextrin showed the same effect on the surface morphology of SD-MPs. This mixture succeeded in suppressing particles shrinkage and collapse owing to the change in their Tg as discussed above. Furthermore, a hard layer on the nano embedded MP surface is formed and was capable to prevent their collapse during the spray drying procedure [20].

3.4 Flow properties

Flow property is considered as one of the promoting parameters for efficient aerosolization of the spray-dried powders. The results for angle of repose, Hausner ratio and Carr's index are shown in detail in (Table S.3-supplementary material). Further, the use of carrier formers enhanced significantly the flow properties compared to spray dried MYR-CPX-SLNs without any carrier (supplementary material). In addition, the combination of maltodextrin with mannitol in SD-MP3/SD-MP4 showed the best flow characteristic as evidenced by low θ, CI and HR values.

3.5 Drug-Excipient Compatibility Study

3.5.1 Differential Scanning Calorimetry (DSC)

DSC analysis was employed to investigate any physical change in the crystalline state and thermal behavior of MYR during the solidification process. The DSC thermograms of raw MYR powder, maltodextrin, mannitol, leucine, selected microparticles formulations (SD-MP2 and SD-MP3) were

depicted in (Figure S.1A-F Supplementary material). It was shown that, no characteristic peak of drug was observed as drug is dissolved in SLNs as previously discussed in our previous work [20] while, peaks of mannitol and leucine were detected after spray drying.

3.5.2 Fourier transform infrared (FTIR) spectroscopy

For further detection of any possible change and chemical interaction between MYR and the SD-MPs in the solid state, IR spectra of MYR, mannitol, maltodextrin, leucine, SD- MPs (SD-MP1-SD-MP3) and spray dried MYR-CPX-SLNs are illustrated in (Figure S.2-Supplementary material). The FT-IR spectrum of SD-MPs showed the disappearance of characteristic MYR peaks. This could be due to overlapping of the drug by the presence of excess carriers. The same observation was exhibited by Ishak and Osman [32], where the characteristic peaks of atorvastatin disappeared in the IR spectrum of spray-dried self-micro emulsifying powders.

3.6 In vitro deposition

For efficient inhalation therapy of lung cancer, the microparticles should be delivered to tumor site with minimum/no exposure to systemic circulation. Accordingly, the aerosol performance of all MP formulae was monitored, and the results are shown in the supplementary material (Figure S.3A)SD-MP3 achieved the most promising aerosolization pattern in line with previously reported formula characterized by MMAD of 2.77 µm, an FPF of 81.23 and an EF of 93% [20]. For the in vivo deposition experiments, fluorescently labeled microparticles were prepared (SD-Cou MP) analogous to formula SD-MP3 but replacing MYR with cou 6. MPs showed an MMAD ~ 2.5 µM, FPF > 80%, and EF > 90%.

4. In vivo Pharmacodynamics (tissue deposition and organ distribution) of fluorescent labeled SLNs & SD-MPs after intravenous and pulmonary administration, respectively

A point of interest is to explore the extent of pulmonary distribution as well as other organ biodistribution following IV and pulmonary oropharyngeal administration of both Lf-coupled and uncoupled labeled SLNs and SD-MPs in addition to free dye as control. Thus, in this section, two factors will be explored, first; the impact of the nanosystem as well as lactoferrin on pulmonary deposition. Second, comparing the two routes of administration *(Local Vs. Systemic)* in terms of the efficiency of in vivo lung deposition. Figures 6 and 7 represent the fluorescent photomicrographs of sections from different organs (Liver, kidney, lung, spleen and brain) 1- and 6h- following IV and pulmonary administration of the aforementioned samples.

Noteworthy, after 1 h, it was found that both IV administered SLNs (Cou-SLNs, Lf-Cou-SLNs) and inhaled nano-embedded microparticles (SD-Cou MP and SD-Lf-Cou MP) showed distinct localization in the bronchial and alveolar tissues (Figure 6A and 7A). This could be accredited to the presence of soy lecithin phospholipids in the SLN composition analogous to pulmonary surfactants phospholipids that might serve as storage bank for the inhaled lipid-based nanosystem [36]. In comparison, control MP and control SLNs loaded with the free dye also demonstrated notable accumulation in the same regions (Figure 6A

&7A). this might be due to lipophilic nature of Coumarin-6, (log P 55.43), which is meant to be subtle across the trachea, airways and alveolar tissue among minutes once insufflation of the dry powder [37].

However, photomicrographs taken after 6 h revealed faster migration of the free dye (Figure 6B & 7B) followed by non-targeted fluorescently-labeled particles (Cou SLNs & SD-Cou MP). This was revealed by the remarkable increase of fluorescent particles in liver, kidney and spleen, while diminished in lungs. Noticeable, functionalizing surface of SLNs with lactoferrin (specific targeting ligand to lungs) (Lf-Cou-SLNs & SD-Lf-Cou MP) showed superior retention in the alveolar cells and protected them from clearance to other organs, which highlights the role of Lf in both targeting and retention [30].

Our results were in agreement with Pandey *et al*. [27] who developed, Lf-functionalized SLNs encapsulating paclitaxel (PTX) for the treatment of lung cancer. The in vivo biodistribution studies showed that concentrations of PTX accumulated in lungs was higher via Lf-SLNs > plain SLNs > free PTX after intravenous administration. These studies suggested that Lf-coupled SLNs could be used as potential targeting carrier for delivering potent drugs directly to the lungs.

In comparison, the local delivery of the free dye via inhalation was expected to place the Cou 6 in the vicinity of lung cells with less systemic exposure resulting in less toxic side effects. But unfortunately, free dye was rapidly cleared from the lung and reached other organs in high concentrations after 6h (Figure 6B). Further, loading Cou 6 into SLNs with/without Lf significantly reduced the dye deposition in other organs relative to free dye, Figure 6B. The enhanced tolerability of Cou-loaded SLNs inhalable MP over the inhalable free Cou MP might be a reason for making the pulmonary delivery of anticancer drugs loaded in nanosystems a viable option and significantly increased the therapeutic effect of the treatment. On the other hand, a higher accumulation of dye was recognized in the liver, kidney and spleen 1 and 6 h after IV administration than local application which might be a reason for organs toxicity associated with systemic application.

As a proof of concept, for more quantitative comparison between pulmonary and IV administration, the mean fluorescence intensity in the photomicrographs was analyzed using Image J software and illustrated in Figures 8A-B. After 1 h, the fluorescence intensity was found to be 259 and 345 gray for SD-Cou MP and SD-Lf-Cou MP, respectively compared to 187.9 and 221.15 gray for Cou-SLNs and Lf-Cou-SLNs. This gives an idea that % of drug deposition in lung after pulmonary administration was ~ 1.5 folds higher than IV injection. However, fading in intensity was noticed after 6 h in case of SD-Cou MP (Figure 8B). This might be related to the fate of SLNs that might be taken by alveolar macrophages which, are responsible for clearance of materials deposited in the alveolar region, in which mucociliary clearance is absent [38,39]. Another explanation could be related to transcytosis of SLNs into the epithelial cells and/or across the epithelia of the respiratory tract into the interstitium and then to blood and lymph might be involved till they reach extra-pulmonary organs [40,41].

This confirmed our findings that by functionalizing surface of SLNs with specific targeting ligand to the lungs aided in maintaining the particles in the lung and protected them from clearance to other organs.

Similarly, the fading in fluorescence intensity in lungs occurred in case of Cou-SLNs while, that of Lf-Cou-SLNs remained almost unchanged (Figure 7A). Therefore, form the previous results it could be concluded that the role of Lf wasn't only exerted on specifying the targeting of nanosystem to lungs in shorter time but also, maintaining it for longer duration and evading their clearance from lungs by macrophages.

Thus, the present study showed that SD-MP loaded with SLNs and coupled with Lf could be effective in treating lung cancer and without targeting ligand, it might have the potential to be used in cancer treatments of organs other than the lung with less invasive procedure than intravenous administration.

Conclusion

The lack of local anti-cancer agents with high safety profile, urges the need for manipulating myricetin, a good candidate for its anticancer, anti-inflammatory and antioxidant potentials, for local treatment of lung carcinoma. It was depicted that, functionalizing of MYR-CPX-SLNs with Lf as target-oriented drug delivery system for the lungs resulted in a remarkable elevation in anti-tumor activity and faster uptake of SLNs by alveolar cancer cells as well. Further, utilizing spray drying technique is a promising approach for preparation of microparticles loaded with MYR-CPX-SLNs. The carrier assembly consisting of mannitol: maltodextrin: leucine at ratio 1.5:0.75:0.75 exhibited a desirable microstructure with good aerosolisation properties for efficient lung deposition evidenced by high emitted fraction values (93 %), % FPF (80.5%) and MMAD (2.81 µm). Overall, the newly developed dry powder system holds a great promise for local delivery of antitumor drug for treatment of lung cancer.

In addition, SD-MP could be effectively used in local treatment of NSCLC as it reached deeply in alveolar cells and maintained in pneumocytes type II. Further, attachment of targeting ligand as Lf prevents the clearance of SLNs to other organs. Thus, the local treatment is more preferred than systemic administration (IV) as it is considered a non-invasive route, thus better patient compliance. Further, it ensures better drug deposition deep in alveolar region than IV, less uptake by macrophages. Furthermore, it offers less drug distribution in other organs which resulted in lower toxicity that is usually accompanied by systemic application.

Abbreviations

MYR (Myricetin), G 50/13 (Gelucire 50/13), Cp (Compritol 888), Lf (Lactoferrin), MYR-PH-CPX (MYR-Phospholipid complex), MYR-CPX-SLNs (MYR-Phospholipid complex loaded solid lipid nanoparticles), Lf-MYR-CPX-SLNs (Lactoferrin coupled-myricetin phospholipid complex loaded solid lipid nanoparticles), Cou-SLNs (coumarin 6-phospholipid complex loaded solid lipid nanoparticles); Lf-Cou-SLNs (Lactoferrin coupled-coumarin 6- phospholipid complex loaded solid lipid nanoparticles) and DMEM (Dulbecco's Modified Eagle's Medium).

Declarations

- **Funding:**

- *The authors declare that no funds, grants, or other support were received during the preparation of this manuscript.*

- **Competing Interests:**

- *The authors have no relevant financial or non-financial interests to disclose.*

- **Author Contributions:**

- *All authors contributed to the study conception and design. The experimental part and data collection were performed by [Dina M. Gaber]. The data analysis, and discussion were carried out by [Dina M. Gaber], [Noha Nafee], [Ahmed O. Elzoghby], and [Osama Y. Abdallah]. The in vivo experiments and the in vitro cellular uptake and colocalization studies were performed by [Dina M. Gaber] and [Maged W. Helmy]. All authors read and approved the final manuscript.*

- **Data Availability:**

- *The datasets generated during and/or analyzed during the current study are available from the corresponding author on reasonable request.*

- **Ethics approval:**

- *The animal study experimental protocol was approved via the Animal Care and Use Committee of the Faculty of Pharmacy, Alexandria University as illustrated in the Supplementary data.*

References

1. Nag MK, Patel S, Panik R, Shrivastava S, Daharwal SJ, Singh MR, et al. Lung Cancer Targeting: A Review. Res J Pharm Technol 2013;6(11):1302–6.
2. Tewabe A, Abate A, Tamrie M, Seyfu A, Abdela Siraj E. Targeted drug delivery—from magic bullet to nanomedicine: principles, challenges, and future perspectives. J Multidiscip Healthc 2021;1711–24.
3. Finbloom JA, Sousa F, Stevens MM, Desai TA. Engineering the drug carrier biointerface to overcome biological barriers to drug delivery. Adv Drug Deliv Rev 2020;167:89–108.
4. Byrne JD, Betancourt T, Brannon-Peppas L. Active targeting schemes for nanoparticle systems in cancer therapeutics. Adv Drug Deliv Rev 2008;60(15):1615–26.
5. Fahmy TM, Fong PM, Goyal A, Saltzman WM. Targeted for drug delivery. Mater Today 2005;8(8, Supplement):18–26.
6. Sahu PK, Mishra DK, Jain N, Rajoriya V, Jain AK. Mannosylated solid lipid nanoparticles for lung-targeted delivery of Paclitaxel. Drug Dev Ind Pharm 2015;41(4):640–9.
7. Mohanta BC, Dinda SC, Palei NN, Deb J. Solid lipid based nano-particulate formulations in drug targeting. Role of novel drug delivery vehicles in nanobiomedicine 2019;95(10.5772).

8. Sarma A, Das MK, Chakraborty T. Ligand Nanoparticle Conjugation Approach for Targeted Cancer Chemotherapy. Nano Medicine and Nano Safety: Recent Trends and Clinical Evidences 2020;377–403.
9. Elzoghby AO, Abdelmoneem MA, Hassanin IA, Abd Elwakil MM, Elnaggar MA, Mokhtar S, et al. Lactoferrin, a multi-functional glycoprotein: Active therapeutic, drug nanocarrier & targeting ligand. Biomaterials 2020;263:120355.
10. Farnaud S, Evans RW. Lactoferrin—a multifunctional protein with antimicrobial properties. Mol Immunol 2003;40(7):395–405.
11. Kell DB, Heyden EL, Pretorius E. The biology of lactoferrin, an iron-binding protein that can help defend against viruses and bacteria. Front Immunol 2020;11:1221.
12. Adlerova L, Bartoskova A, Faldyna M. Lactoferrin: a review. Vet Med (Praha) 2008;53(9):457–68.
13. Luzi C, Brisdelli F, Iorio R, Bozzi A, Carnicelli V, Di Giulio A, et al. Apoptotic effects of bovine apo-lactoferrin on HeLa tumor cells. Cell Biochem Funct 2017;35(1):33–41.
14. Jiang R, Lönnerdal B. Bovine lactoferrin and lactoferricin exert antitumor activities on human colorectal cancer cells (HT-29) by activating various signaling pathways. Biochem Cell Biol 2017;95(1):99–109.
15. Shilpi S, Vimal VD, Soni V. Assessment of lactoferrin-conjugated solid lipid nanoparticles for efficient targeting to the lung. Prog Biomater 2015;4(1):55–63.
16. Gibbons JA, Kanwar RK, Kanwar JR. Lactoferrin and cancer in different cancer models. Front Biosci(Scholar edition) 2010;3:1080–8.
17. Elfinger M, Maucksch C, Rudolph C. Characterization of lactoferrin as a targeting ligand for nonviral gene delivery to airway epithelial cells. Biomaterials 2007;28(23):3448–55.
18. Elsayed I, AbouGhaly MHH. Inhalable nanocomposite microparticles: preparation, characterization and factors affecting formulation. Expert Opin Drug Deliv 2016;13(2):207–22.
19. Yang Y, Cheow WS, Hadinoto K. Dry powder inhaler formulation of lipid–polymer hybrid nanoparticles via electrostatically-driven nanoparticle assembly onto microscale carrier particles. Int J Pharm 2012;434(1):49–58.
20. Nafee N, Gaber DM, Elzoghby AO, Helmy MW, Abdallah OY. Promoted Antitumor Activity of Myricetin against Lung Carcinoma Via Nanoencapsulated Phospholipid Complex in Respirable Microparticles. Pharm Res 2020;37(82):1–24.
21. Gaber DM, Nafee N, Abdallah OY. Myricetin solid lipid nanoparticles : Stability assurance from system preparation to site of action. Eur J Pharm Sci 2017;109(May):569–80.
22. Nafee N, Husari A, Maurer CK, Lu C, Rossi C De, Steinbach A, et al. Antibiotic-free nanotherapeutics : Ultra-small , mucus-penetrating solid lipid nanoparticles enhance the pulmonary delivery and anti-virulence efficacy of novel quorum sensing inhibitors. JCR;2014;192:131–40.
23. Roa WH, Azarmi S, Al-Hallak MHDK, Finlay WH, Magliocco AM, Löbenberg R. Inhalable nanoparticles, a non-invasive approach to treat lung cancer in a mouse model. JCR 2011;150(1):49–55.

24. Yang M, Jiang D, Chen Z, Chen J. Photodynamic therapy of drug-resistant human colon adenocarcinoma using verteporfin loaded TPGS nanoparticle with tumor homing and penetrating peptide functionalized. RSC Adv 2016;6:100984–92.
25. Stor S. In vivo biodistribution of fluorescent nanocolloids intended for drug delivery . Evaluation of PEGylation state and fluorophore incorporation approach . 2012;
26. Yao X, Bunt C, Cornish J, Quek S, Wen J. Preparation, optimization and characterization of bovine lactoferrin-loaded liposomes and solid lipid particles modified by hydrophilic polymers using factorial design. Chem Biol Drug Des 2014;83(5):560–75.
27. Pandey V, Gajbhiye KR, Soni V. Lactoferrin-appended solid lipid nanoparticles of paclitaxel for effective management of bronchogenic carcinoma. Drug Deliv 2015;22:199–205.
28. Kurmi BD, Gajbhiye V, Kayat J, Jain NK. Lactoferrin-conjugated dendritic nanoconstructs for lung targeting of methotrexate. J Pharm Sci 2011;100(6):2311–20.
29. Rajendran P, Maheshwari U, Muthukrishnan A, Muthuswamy R, Anand K, Ravindran B, et al. Myricetin: Versatile plant based flavonoid for cancer treatment by inducing cell cycle arrest and ROS–reliant mitochondria-facilitated apoptosis in A549 lung cancer cells and in silico prediction. Mol Cell Biochem 2021;476(1):57–68.
30. Liu BR, Huang YW, Aronstam RS, Lee HJ. Identification of a short cell-penetrating peptide from bovine lactoferricin for intracellular delivery of DNA in human A549 cells. PloS One 2016;11(3):e0150439.
31. Malamatari M, Somavarapu S, Bloxham M, Buckton G. Nanoparticle agglomerates of indomethacin: The role of poloxamers and matrix former on their dissolution and aerosolisation efficiency. Int J Pharm 2015;495(1):516–26.
32. Ishak RAH, Osman R. Lecithin/TPGS-based spray-dried self-microemulsifying drug delivery systems: In vitro pulmonary deposition and cytotoxicity. Int J Pharm 2015;485(1–2):249–60.
33. Osman R, Kan PL, Awad G, Mortada N, Abd-Elhameed ES, Alpar O. Spray dried inhalable ciprofloxacin powder with improved aerosolisation and antimicrobial activity. Int J Pharm 2013;449(1):44–58.
34. Kumar S, Gokhale R, Burgess DJ. Sugars as bulking agents to prevent nano-crystal aggregation during spray or freeze-drying. Int J Pharm 2014;471(1):303–11.
35. Cruz L, Fattal E, Tasso L, Freitas GC, Carregaro AB, Guterres SS, et al. Formulation and in vivo evaluation of sodium alendronate spray-dried microparticles intended for lung delivery. JCR 2011;152(3):370–5.
36. Fehrenbach H. Alveolar epithelial type II cell: defender of the alveolus revisited. Respir Res 2001;2(1):33.
37. Lombry C, Bosquillon C, Préat V, Vanbever R. Confocal imaging of rat lungs following intratracheal delivery of dry powders or solutions of fluorescent probes. JCR 2002;83(3):331–41.
38. Yang W, Peters JI, Williams RO. Inhaled nanoparticles-A current review. Int J Pharm 2008;356(1–2):239–47.

39. Olsson B, Bondesson E, Borgström L, Edsbäcker S, Eirefelt S, Ekelund K, et al. Pulmonary drug metabolism, clearance, and absorption. In: Controlled Pulmonary Drug Delivery. Springer; 2011. page 21–50.
40. Zhang J, Wu L, Chan HK, Watanabe W. Formation, characterization, and fate of inhaled drug nanoparticles. Adv Drug Deliv Rev 2011;63(6):441–55.
41. Todoroff J, Vanbever R. Fate of nanomedicines in the lungs. Curr Opin Colloid Interface 2011;16(3):246–54.

Figures

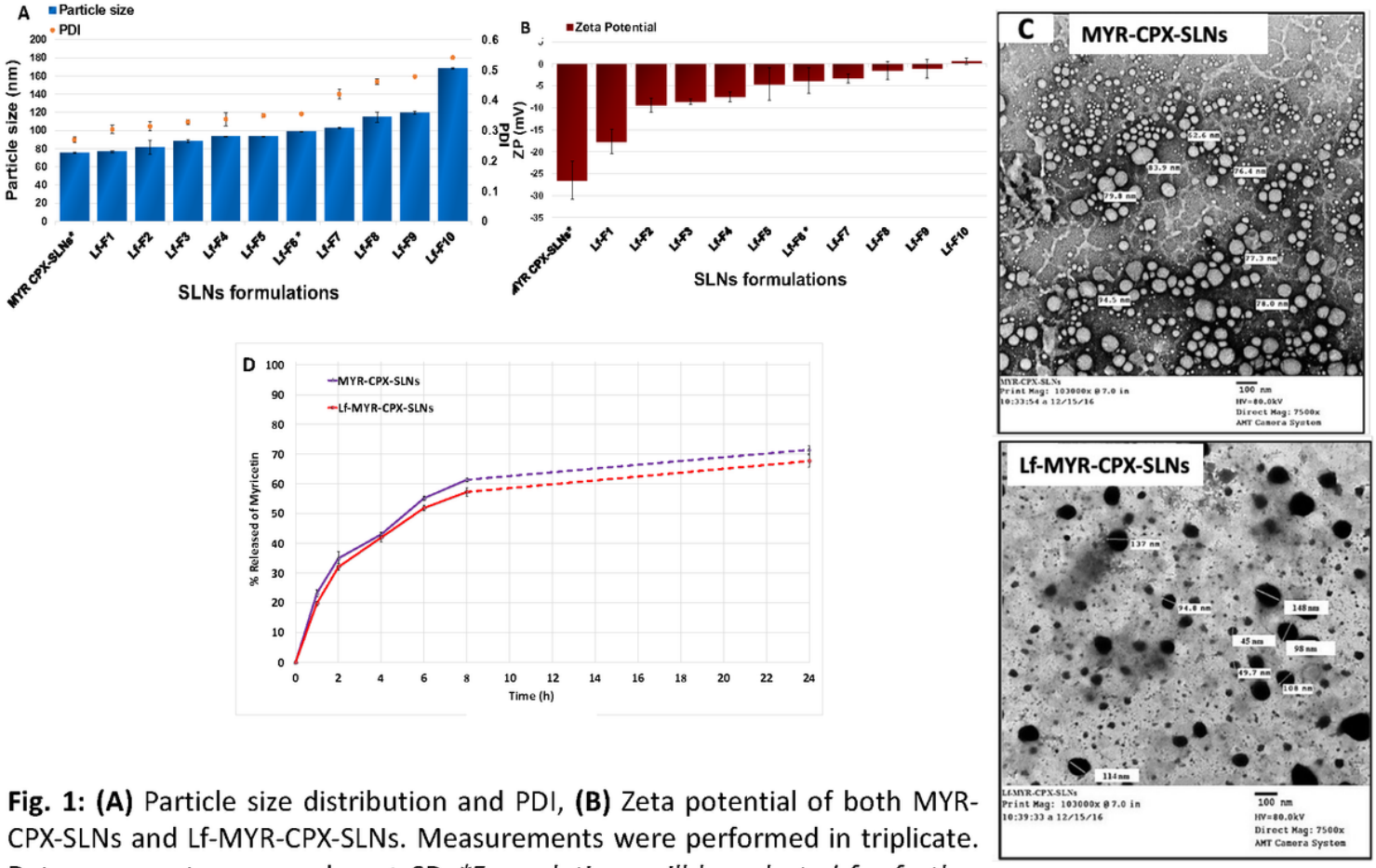

Fig. 1: (A) Particle size distribution and PDI, **(B)** Zeta potential of both MYR-CPX-SLNs and Lf-MYR-CPX-SLNs. Measurements were performed in triplicate. Data represents mean values ± SD, **Formulations will be selected for further evaluation*, **(C)** TEM microphotograph of: MYR-CPX-SLNs and Lf-MYR-CPX-SLNs, **(D)** In vitro release of MYR from: MYR-CPX-SLNs, and Lf-MYR-CPX-SLNs in water/ethanol (1:1). Each point represents the mean (n=3) ± SD.

Figure 1

See image above for figure legend

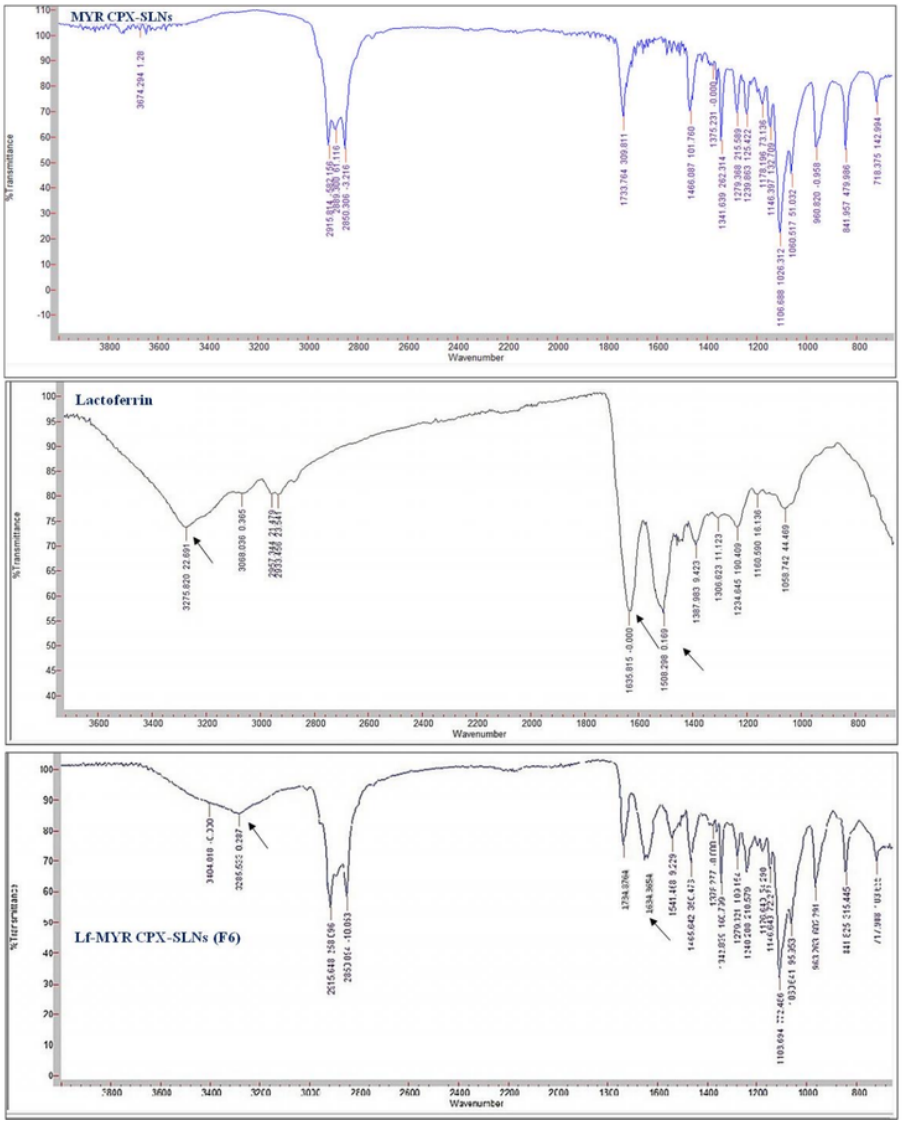

Fig. 2: FTIR spectra of MYR-CPX-SLNs, lactoferrin and Lf-MYR-CPX-SLNs (F6).

Figure 2

See image above for figure legend

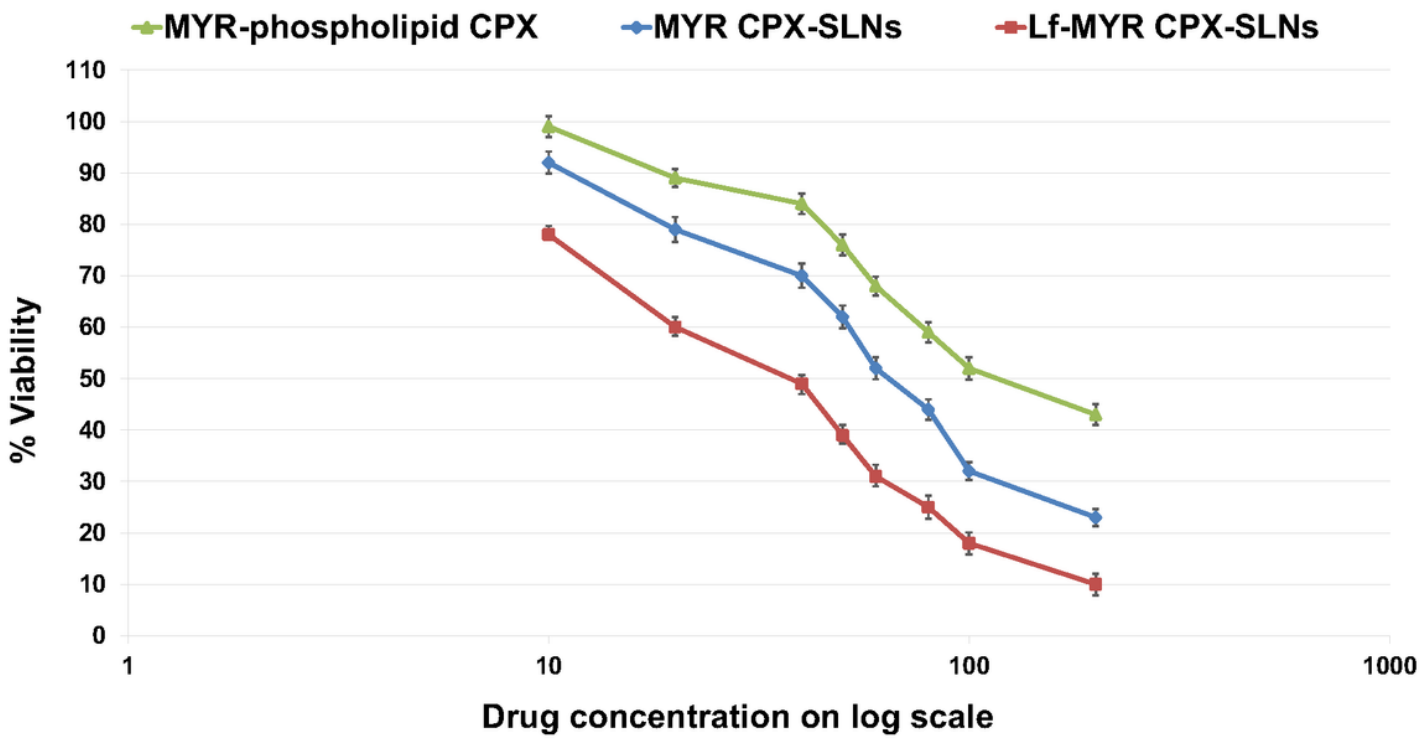

Fig. 3: Percentage of viability of A549 cells measured by the MTT viability assay after exposure for 24 h to various concentrations of MYR-phosholipid CPX, MYR-CPX-SLNs and Lf-MYR-CPX-SLNs at 37± 0.5°C, mean ±SD., (n = 3).

Figure 3

See image above for figure legend

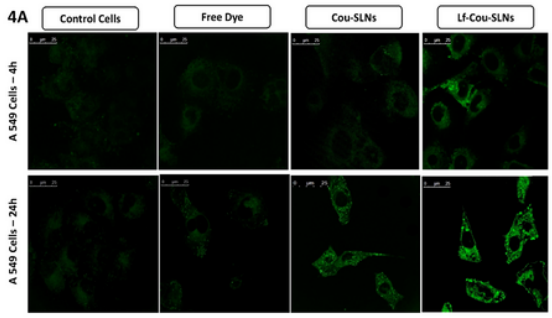

Fig. 4A: Confocal laser microscopy images of A549 cells incubated with free cou solution, Cou-SLNs and Lf-Cou-SLNs (magnification 63×). After 4 and 24 h incubation with a suspension of cou 6 (Green)-containing SLNs (40 and 50 mg/ml) for Cou-SLNs and Lf-Cou-SLNs, respectively at 37 °C. Scale bar, 25 µm.

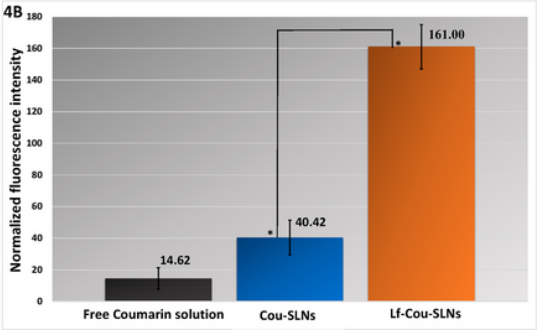

Fig. 4B: Fluorescence intensity recovered from A549 viable cells after treatment with free dye, Cou-SLNs or Lf-Cou-SLNs. Measurements of the fluorescence intensity were performed 24 h post-treatment. Statistically significant differences from Lf-Cou-SLNs and Cou-SLNs to untreated cells ($p<0.05$).

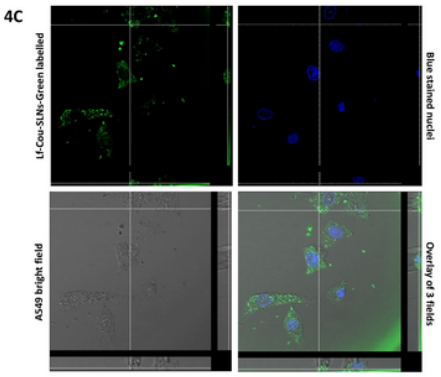

Fig. 4C: CLSM images of the cellular uptake of Lf-Cou-SLNs in A549 lung cancer cells after 24 h. Scale bar, 25 µm.

Figure 4

See image above for figure legend

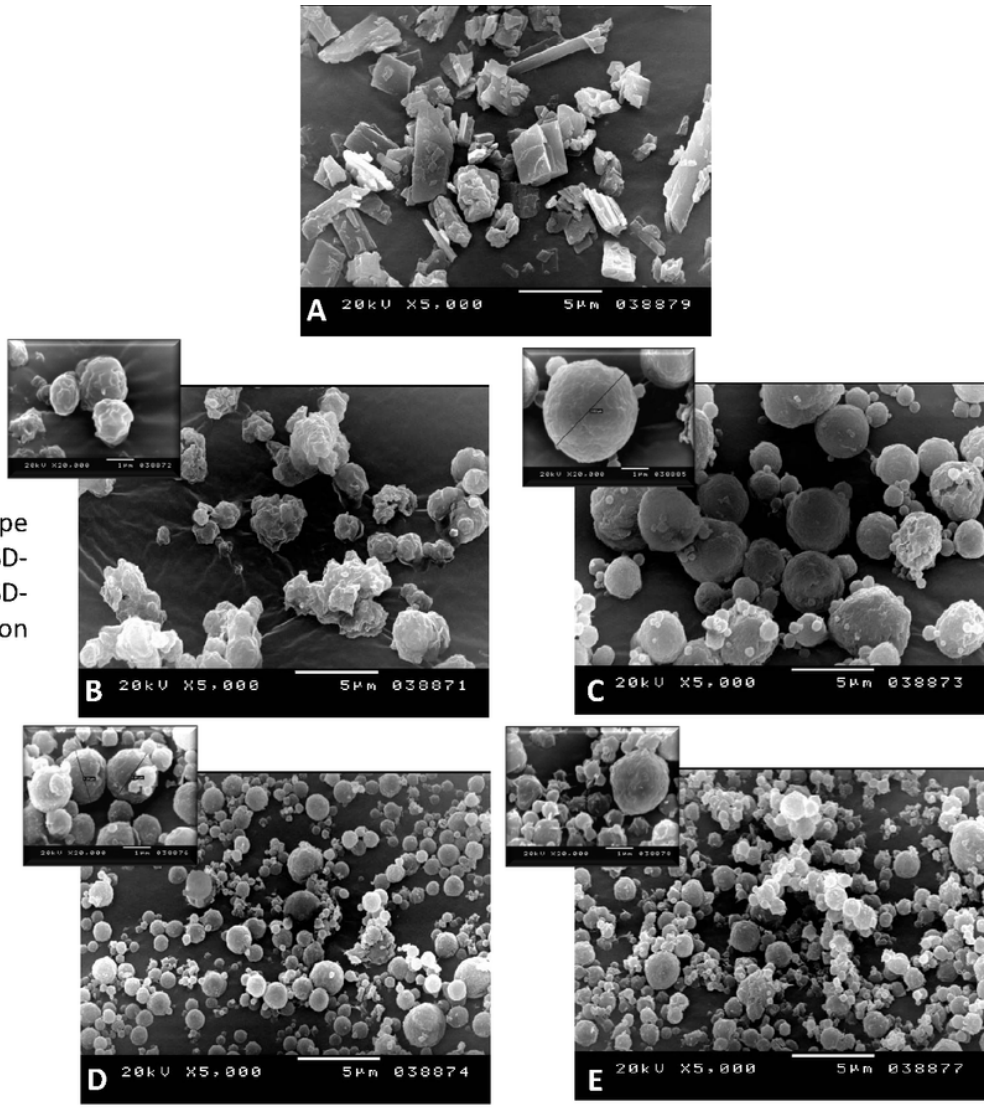

Fig. 5: Scanning electron microscope (SEM) micrograph of; **(A)** MYR, **(B)** SD-MP1, **(C)** SD-MP2, **(D)** SD-MP3, (E) SD-MP4, at intermediate magnification power 5000X.

Figure 5

See image above for figure legend

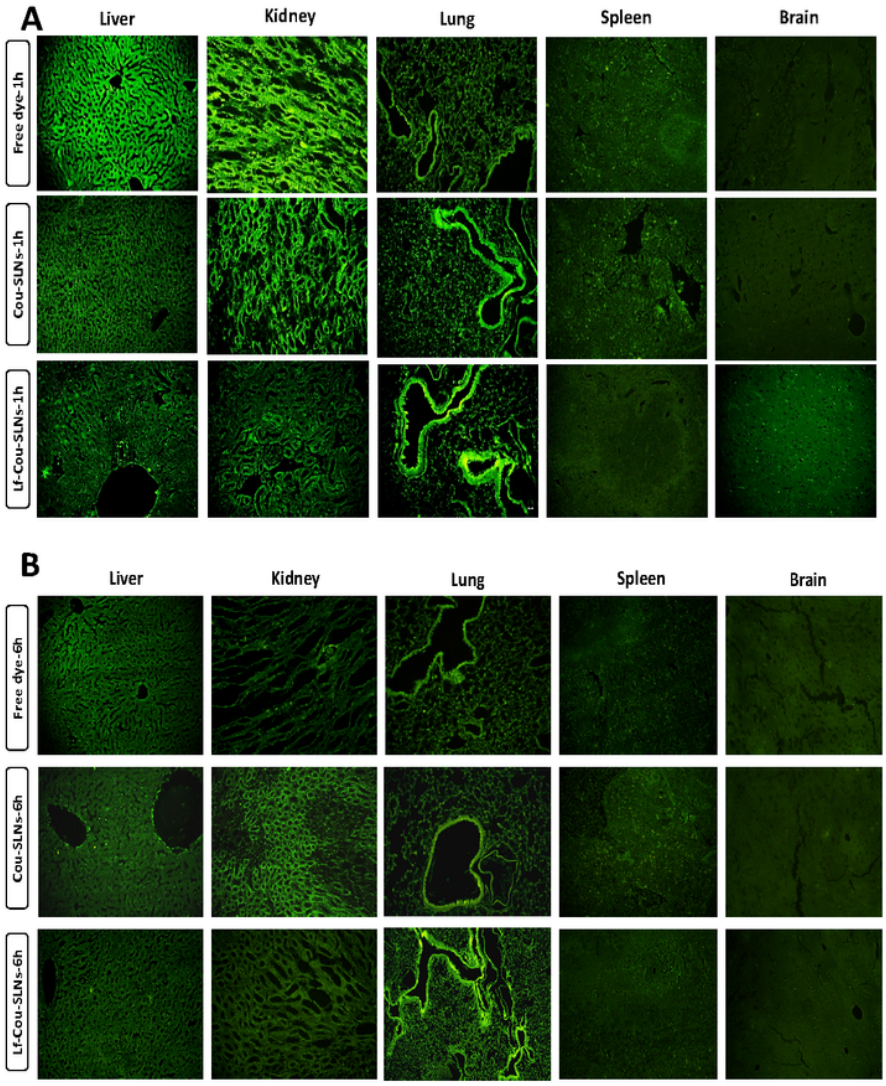

Fig. 6: Fluorescence photomicrographs of different organs tissues (A) 1h, (B) 6h following the intravenous administration of; Free dye solution, Cou-SLNs, and Lf-Cou-SLNs. (Magnification power 20X).

Figure 6

See image above for figure legend

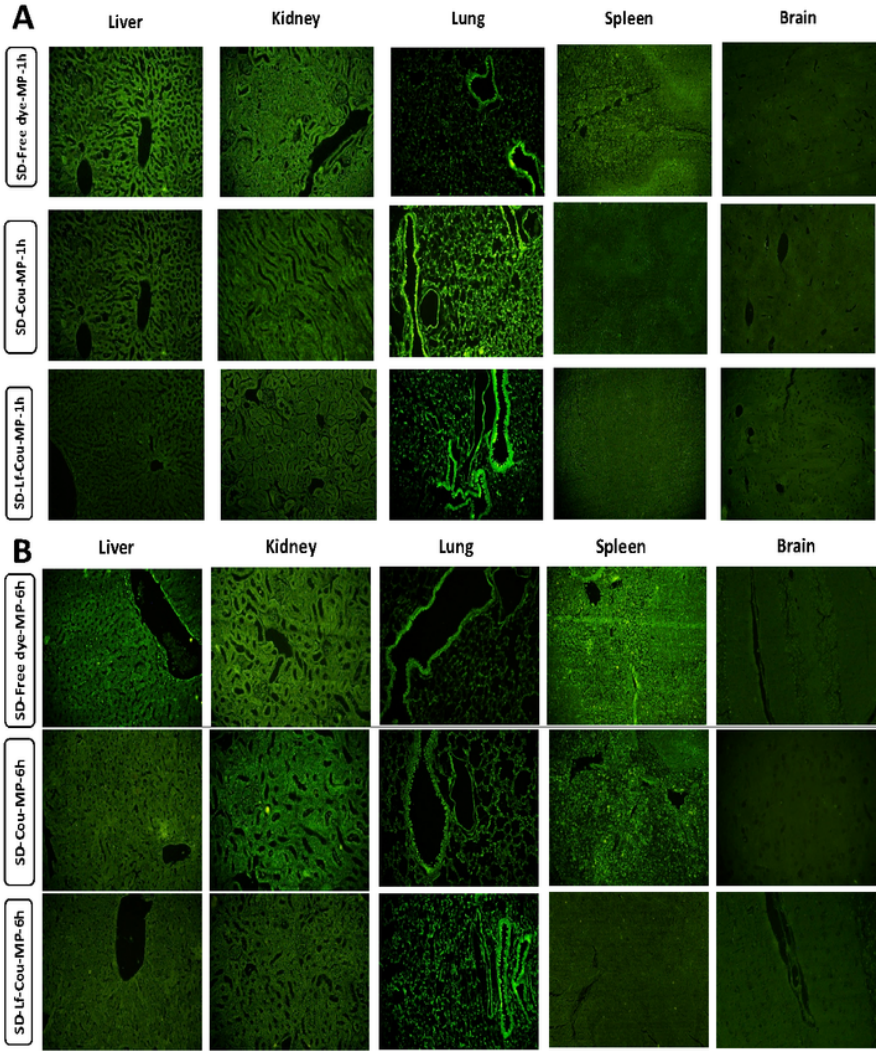

Fig. 7: Fluorescence photomicrographs of different organs tissues (A) 1h, (B) 6h following the pulmonary administration of; SD-Free dye MP, SD-Cou MP, and SD-Lf-Cou MP. (Magnification power 20X).

Figure 7

See image above for figure legend

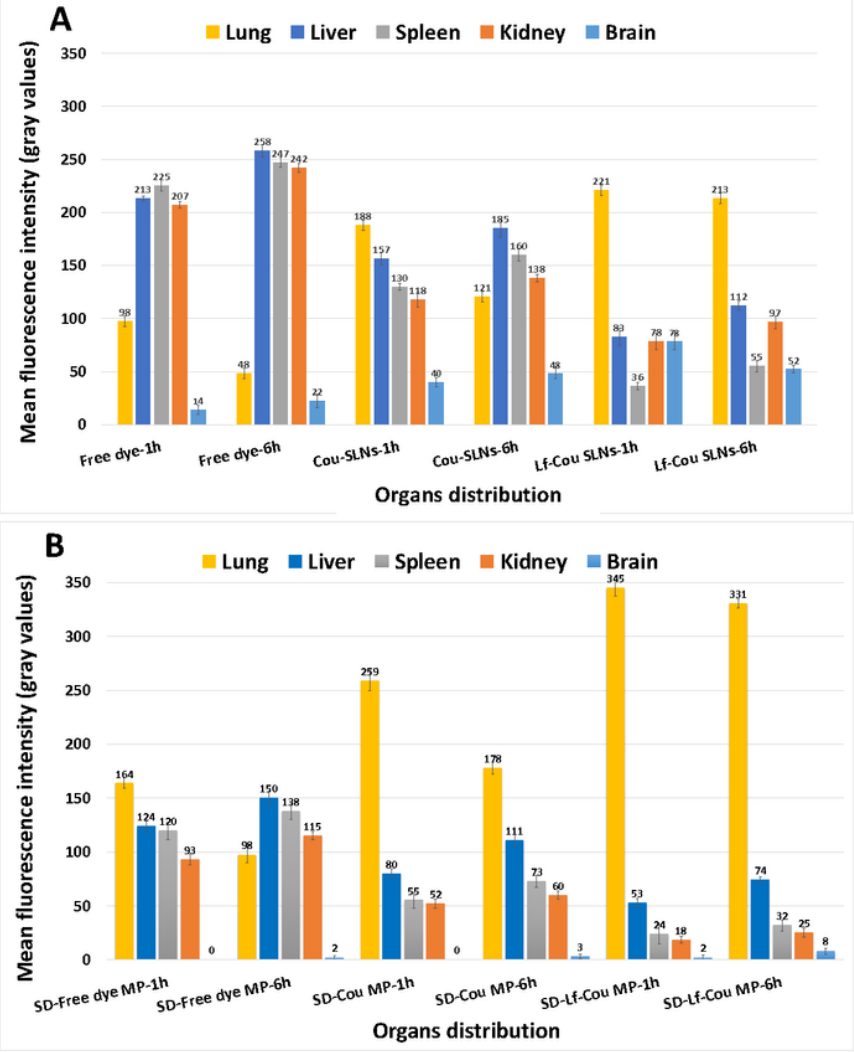

Fig. 8: Fluorescent intensity after (A) IV, and (B) pulmonary administration of free dye, Cou-SLNs and Lf-Cou-SLNs were detected in the tissue organs 1 and 6 h post pulmonary administration.

Figure 8

See image above for figure legend

Supplementary Files

This is a list of supplementary files associated with this preprint. Click to download.

- floatimage1.png
- GaberetalLFMYRSLNsSupplementarymaterialDDTR.docx